Proceedings of IMECE04
2004 ASME International Mechanical Engineering Congress and Exposition
November 13-20, 2004, Anaheim, California USA

IMECE2004-60465

REAL-TIME ADAPTIVE MODELING APPROACH TO COMPENSATE THE THERMAL DEFORMATION OF NONLINEAR MACHINE TOOL STRUCTURES

S. Fraser
Senior Control Systems Engineer, LHP Software LLC, Columbus, Indiana, USA

Helmi Attia, FASME
Aerospace Manufacturing Technology Center, Institute for Aerospace Research, National Research Council of Canada/ McGill University, Montreal, Quebec, Canada

M. O. M. Osman, FASME
Mechanical Engineering Department, Concordia University, Montreal, Quebec, Canada

ABSTRACT

Machine tool structures cannot be fully optimized at the design stage to cover the wide range of operating conditions. Therefore, reliable control systems emerge as the logical solution to compensate for thermal errors. Due to the difficulty of measuring the relative thermal displacement δ between the tool and the workpiece during machining, δ has to be accurately estimated in real-time. A new concept of adaptive modeling is introduced to develop control-based dynamic models to predict and compensate for thermal deformation of *nonlinear* complex machine tool structures. A key element of this approach is to replace the changes in the contact pressures along the joint by fictitious contact heat sources FCHS. This allows us to track the system nonlinearity through temperature measurements and real-time inverse heat conduction IHCP solution. The proposed approach dealt successfully with a number of challenges; namely, the non-uniqueness of the problem, and the lack of sufficient conditions to identify each of such unusual FCHS separately. The results showed that the models are capable of satisfying the accuracy, stability and computational efficiency requirements, even when the temperature measurement signal is contaminated with random noise. The results also showed that the thermal deformation transfer function behaves as low-pass filters, and as such it attenuates the high frequency noise associated with temperature measurement error.

KEYWORDS

Nonlinear structures, machine tools, thermal deformation, control, compensation, inverse heat conduction

INTRODUCTION

Management of thermal effects associated with high cutting speeds and federates is a focal point for a number of emerging technologies; namely, high speed and high precision machining. The problem of thermal deformation of machine tool structures is becoming, therefore, more critical than ever. Control systems based on inductive and deductive approaches were developed over the years to circumvent the difficulty of measuring the relative thermal displacement vector $\delta(t)$ between the tool and the workpiece during machining. In the inductive approach, indirect displacement or temperature measurements [1-4] are used to estimate $\delta(t)$ and to activate a control system. This approach is not reliable since deformation prediction is not uniquely defined and relies on an empirical base function that bears no physical similarity to the actual phenomena. In the deductive approach, numerical models are used to fully describe the heat transfer and deformation processes [5,6]. The inherent deficiency of this approach is a result of being either inaccurate or too slow to be used in real-time control applications. Moreover, the magnitudes of the heat sources are not updated during operation.

In response to the problems associated with both the empirical and numerical approaches, the authors of this paper have recently introduced the theory of *generalized modelling* and proposed integrating it into a new control system [7]. This approach ensures the complete analytical description of the thermal and deformation processes, and the construction of the thermal and deformation transfer functions that are calibrated from the step response of the real structure [8]. The control system incorporates a real-time inverse heat conduction problem IHCP solver to estimate the heat input to the structure

Copyright © 2004 by ASME

Downloaded From: https://proceedings.asmedigitalcollection.asme.org on 07/01/2019 Terms of Use: http://www.asme.org/about-asme/terms-of-use

q(t) [9]. With the s-domain representation of the dynamic thermoelastic models, the design and performance of the control system can be optimized [10,11]. The theory on *generalized modeling* was formulated in such a way that it can directly be applied to any machine tool structure without further analytical development or modelling by the end user.

The main limitation of this effort, however, is that it does not account for the nonlinear thermoelastic behaviour of the structure, and non-stationary heat sources. To extend the generalized modeling approach to these applications, a new IHCP solution was developed [12] to deal with the thermal inertia and delayed response. In the present work, a new concept of adaptive modeling is introduced to allow real-time estimation of thermal deformation of *nonlinear* machine tool structures that may result from the thermoelastic closed loop interactions introduced by structural joints [13-15].

THEORY OF GENERALIZED MODELING

Inverse Thermal Problem

The concept of *generalized modeling*, which was introduced in [7], is based on the premise that a complex process that has no analytical description can be approximated by the analytical solution to a similar, but yet simpler, phenomenon which is physically related. Then, by examining the behavior of this analytical solution, it is possible to identify the mathematical features and attributes of the real process and to construct a physics-based model that can be calibrated from the step response of the real system. To satisfy the conditions of mathematical similarity between the fundamental and the real problems, the two problems should be physically similar in nature, formulation, boundary conditions, and initial conditions.

The box-shaped structural components of a typical machine tool can be visualized as if its walls are bent out flat into a large thin plate of uniform thickness 'w', assuming that the internal ribs and brackets do not greatly alter the mathematical structure of the solution. Heat sources take a variety of shapes and sizes, but they can be adequately represented in the simplified model as a circular ring of heat generation of radius r_0. These assumptions were extensively validated in [7-12] and proved to be justifiable. The general solution of this fundamental problem was derived in [7] using Hankel transformation:

$$T(r,t) = \frac{\alpha}{2\pi kw}\int_0^{\infty} \beta\, J_0(\beta r)\, J_0(\beta r_0)\, e^{-(a+\beta^2)\alpha t} \int_0^{t} q(\tau)\, e^{-(a+\beta^2)\alpha t}\, d\tau d\beta \quad (1)$$

where k and α are the material thermal conductivity and diffusivity, respectively, while the function $J_0(...)$ is the Bessel function of the zeroth order. If the heat generation $q(\tau)$ is taken to be a step function of magnitude q, then the following equation for the generalized temperature step response $T_s(r,t)$, at point r and time t, is obtained [7]:

$$T_s(r,t) = K\, q \int_0^{\infty} \frac{\beta}{\beta^2 + a}\, J_0(\beta r)\, J_0(\beta r_0) \left[1 - e^{-(a+\beta^2)\alpha t}\right] d\beta \quad (2)$$

where $K=1/(2\pi kw)$. The four lumped parameter K, a, α and r are determined through off-line calibration of the step response of the real structure, using a non-linear optimization scheme. The value of r_0 is chosen arbitrarily rather than calibrated because it was found that the calibration of the other parameters gives sufficient flexibility and thus the fifth parameter is redundant. Since the calibrated step response function is to be used to determine the unknown time variation of the heat input to the real machine tool structure in real-time, special consideration should be given to the effect of other heat sources on $T_s(r,t)$. By taking the temperature difference ΔT between two points near the heat source, this interaction is eliminated. In addition, the fluctuation in ambient temperature and the systematic temperature measurement errors are compensated for [9]. It was proven [9] that mathematical structure of Eq. 2 is equally applicable to $\Delta T_s(t)$, provided that the distance between the measurement points is not excessively large; a condition that can easily be met. Therefore, $\Delta T_s(t)$ is used for calibrating the lumped parameters K, a, α and r_0.

Transformation of the function $\Delta T_s(t)$ into the s-domain allows us to obtain the transfer function G(s) of the inverse heat conduction problem IHCP [12] even when the thermal inertia of the structure is significant:

$$G(r,s) = \frac{Q(s)}{\Delta T_s(s)} = \frac{1}{K\alpha \int_0^{\infty} \frac{\beta\ J_0(\beta r)\ J_0(\beta r_0)}{s + [a+\beta^2]\alpha} d\beta} \quad (3)$$

where s is the Laplacian operator, s=R+Ij, and the heat input corresponding to this step response is Q(s)=q/s. During operation, the time-dependent heat input to the machine tool structure is obtained in the s-domain from the temperature difference measurement $\Delta T(t)$ at the same points used in the calibration of Eq. 2:

$$Q(s) = G(r,s)\ \Delta T(s) \quad (4)$$

Real-time solution of the IHCP in the time domain is obtained through the following convolution integration:

$$Q(t) = \int_0^{t} G(r, t-\tau)\, \Delta T(\tau)\, d\tau \quad (5)$$

The IHCP solution given by Eq. 5, requires off-line numerical transformation of G(r,s), expressed by Eq. 3, from the s-domain to the t-domain:

$$G(r,t) = \frac{1}{2\pi j} \int_{\sigma-j\infty}^{\sigma+j\infty} e^{st}\, G(r,s)\, ds \quad (6)$$

where σ is a real number that is larger than the largest pole of G(r,s). The transformation process poses a significant challenge in terms of the truncation error and computational inefficiency, due to the following factors:

Copyright © 2004 by ASME

Downloaded From: https://proceedings.asmedigitalcollection.asme.org on 07/01/2019 Terms of Use: http://www.asme.org/about-asme/terms-of-use

1. The need to evaluate the integrand in Eq. 3 for $0<I,R<\infty$.
2. The integration of Eq. 6 has to be carried out numerically, since no closed form solution is available.
3. The integrand is oscillatory and decays very slowly.
4. The presence of singularity functions in the G(r,s) expression.

These problems were fully addressed and resolved in the analysis recently presented in [12], by modifying the mathematical form of the decaying part of the integrand in Eq. 3, and by introducing regularization *function* f_R to the step response function $\Delta T_s(t)$:

$$f_R = (At + Bt^2)\, e^{-\gamma t} \qquad (7)$$

The method of determining the parameters A, B and γ in Eq. 7 is discussed in [12]. It should be noted that the regularization process allows us to eliminate higher order singularities and to deal with the *delay* in the step response, which is inevitable when the heat source is not close enough to the points where temperature measurement are taken. This particular issue is critical to the formulation of the thermal deformation process in nonlinear structures as will be shown in section .3.

Thermal Deformation Problem

From the experimental results [11] and the FE analyses that were conducted for different operating conditions, the thermal deformation at various points on the structure $\delta(x,y,z,t)$ is found to be always *over-damped*. This observation is consistent with conclusion drawn by Attia et al. [13], which is based on system analysis of linear machine tool systems. The mathematical description of this process can therefore be of the following linear model:

$$\delta(t) = C + D - Ce^{-ct} - De^{-dt} + Ete^{-et} \qquad (8)$$

This model ensures that $\delta(t=0) = 0$, and accommodates initial delays; $d\delta/dt = 0$, at t=0. The analytical form of Eq. 8, with six parameters C, D, E, c, d and e, was found to be sufficiently accurate to describe linear machine tool systems. As in the thermal model, these parameters are determined from the calibration of the step response of the structure.

THERMAL DEFORMATION OF NONLINEAR MACHINE TOOL STRUCTURES

Theory of Nonlinear Thermoelastic Behaviour of Structural Joints

The theory on the nonlinear thermoelastic behaviour of structural joints, developed by Attia and Kops [14,15], provides the conceptual framework for developing adaptive generalized models to control the thermal deformation of nonlinear structures. This theory is based on the recognition of the role of the joint in introducing a thermo-mechanical closed-loop interaction between the following three elements (Fig. 1): the contact pressure distribution along the joint, the corresponding thermal contact resistance distribution, and the thermal deformation of the structure. These elements are interconnected by: the temperature field, the thermal stresses generated along the joint, and the contact configuration on both the micro- and macro-scale. The figure shows clearly that the changes in the contact pressures distribution is both controlling and being controlled by the thermal deformation of the machine tool structure [16]. Depending on the machine tool design and the location of the heat sources, the effect of nonlinearity could be significant enough to cause the structure to behave as a second order system instead of a first order system [13], had the joint effect not considered. This causes the nonlinear machine structure to be behaves as under-damped system. Computer simulation of the nonlinear thermoelastic behaviour of structural joints requires expressing the thermal contact resistance R_c of the structural joint in terms of the local contact pressure p_n and the properties of contacting surfaces.

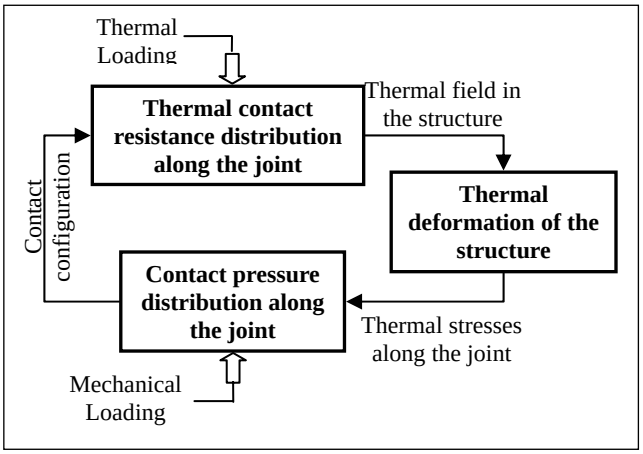

Figure 1: Nonlinear thermoelastic closed-loop interactions introduced by the structural joint

Thermal Contact Resistance of Structural Joints

Due to the nature of surface topography, contacting bodies transmit load through discrete 'micro-contact' areas that are usually clustered within a smaller number of bounded zones known as the 'contour areas' or the 'macro-contacts'. As the heat flow lines approach the contact zone, they tend to converge towards the least resistance paths, giving rise to the known 'thermal constriction resistance'. Therefore, the total heat flow will be divided into a number n_1 of separate channels which correspond to the macroscopic constriction resistance R_{MAC} in the contact region, and the gap resistance R_G in the non-contact region. Microscopic constriction resistances R_{mic} and interstitial fluid resistances R_f are subsequently created as each of the heat flow channels is subdivided again into a number n_2 of microscopic heat flow channels, each correspond to a single micro-contact and its surrounding interstitial fluid. Microscopic and macroscopic constriction resistances can be added together to determine the overall thermal contact resistance R_C:

Copyright © 2004 by ASME

Downloaded From: https://proceedings.asmedigitalcollection.asme.org on 07/01/2019 Terms of Use: http://www.asme.org/about-asme/terms-of-use

$$R_c = \left[\sum_{i=1}^{n_1} \left(\frac{1}{R_G} + \frac{1}{R_{MIC} + R_{MAC}} \right)_i \right]^{-1} \quad (9)$$

Attia et al. reported that the thermal contact resistance is dominated by the microscopic component R_{MIC} [15] and therefore Eq. 9 can be simplified by ignoring the R_G and R_{MAC} terms. Assuming that the n_2 isothermal micro-contact areas have an average radius 'a' and are thermally connected, then the thermal contact resistance is defined as:

$$R_c = R_{MIC} = \left[\sum_{j=1}^{n_2} \left(\frac{1}{R_f} + \frac{1}{R_{mic}} \right)_j \right]^{-1} \quad (10)$$

For normally distributed surface asperities, the contact resistance R_c is reduced further to the following expression [17] when the interstitial fluid resistance is ignored:

$$R_c = \left[C \left(\frac{\overline{m}}{\overline{\sigma}} \right) k_h \left(\frac{p_n}{H_B} \right)^{0.985} \right]^{-1} \quad (11)$$

where C is a constant, k_h is the harmonic thermal conductivity of the contacting solids; $k_h = 2k_1 k_2 / (k_1 + k_2)$, $\overline{m}$ is the mean of absolute slope of surface asperities, $\overline{\sigma}$ is the equivalent standard deviation of contacting asperities, p_n is the normal contact pressure, and H_B is the hardness of the softer material.

Adaptive Thermoelastic Model of Nonlinear Machine Tool Structures

A block diagram representing the real-time modeling of a nonlinear machine tool structure is shown in Fig. 2. In order to reproduce the closed-loop thermoelastic interactions introduced by the structural joint, the parameters of the thermal and deformation models should be modified in accordance with the actual contact pressure distribution, as shown by the dotted line connections in Fig 2. Implementation of such an adaptive model in this case requires pre-knowledge of the relationship between the contact pressure distribution and the parameters of the thermal and deformation models.

Practically, this is an impossible due to the following two major obstacles. First, the relationship between the coefficients of the deformation model (Eq. 8) and the contact pressure would have to be determined experimentally, by varying the contact pressure distribution and then recalibrating the coefficients of the model. Second, the adaptive model requires a real time estimate of the contact pressure, which cannot directly be measured in a real machine tool in operation. Thus, while the adaptive approach is useful for visualization, it is not a practical solution that could be implemented in real-time. (x)

In order to achieve a realizable solution, the dotted line connections in Fig 2 are replaced by the double lines connecting the thermal deformation model to temperature measurements. In addition to the temperature measurement set T_{j1} used to solve the IHCP to estimate the heat input to the structure, there is another measurement set T_{j2} that is used to estimate the contact pressure distribution. This scheme provides a mechanism for indirectly estimating the contact pressure distribution from temperature measurements. The problem which remains to be solved is how to establish a reliable model relating measured temperatures to the contact pressure distribution. This relationship is not an obvious one since the temperature, even in the vicinity of the source, depends on factors other than the contact pressure. Furthermore, the adaptive model does not lend itself easily to empirical type models whose calibration requires the availability of known input and output data. In the next sections, the generalized modeling theory is developed further to provide a feasible solution for the nonlinear adaptive model.

The Concept of Fictitious Contact Heat Source

Rationale and Theoretical Considerations

Equation 11 shows that the joint thermal contact resistance is governed by R_{MIC}, which is inversely proportional to the contact pressure. Therefore, the effect of the developing compressive thermal contact stresses over an area of the structural joint is to increase the heat flux through this area. The reverse is true over the areas that are subject to tensile

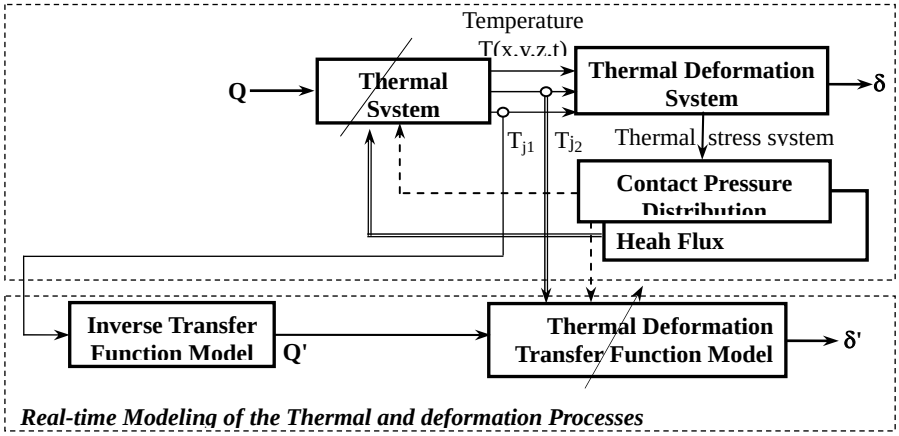

Figure 2: Block diagram of an adaptive model of the thermal deformation of nonlinear machine tool system

Copyright © 2004 by ASME

Downloaded From: https://proceedings.asmedigitalcollection.asme.org on 07/01/2019 Terms of Use: http://www.asme.org/about-asme/terms-of-use

stresses. Therefore, the thermoelastic nonlinearity of the system can be viewed as a continuous re-distribution of the heat flux along the joint, until the steady state is reached. This suggests that the *change* in the distribution of the contact pressure δp_n over the joint can be replaced by a series of fictitious contact heat sources FCHS (or sinks), each channeling the local incremental heat flux ∂q. The sign of ∂q is positive or negative, depending on whether the thermal contact stresses at this location are compressive or tensile, respectively.

The equivalence of ∂p_n and ∂q can be approached from a different angle. To overcome the interface thermal contact resistance R_c, a temperature drop ΔT has to be established across the interface to conduct heat flow rate q:

$$q = \frac{\Delta T}{R_c} \tag{12}$$

Since R_c is proportional to the inverse of the contact pressure p_n (Eq. 11), then:

$$q \propto p_n \, \Delta T \tag{13}$$

Therefore, the nonlinear deviation in the heat flux ∂q can be expressed as:

$$\partial q \propto \partial p_n \, \Delta T \tag{14}$$

where ∂p_n is the *change* in the contact pressure from that of the corresponding linear system.. If ΔT is assumed to be nearly constant, then:

$$\partial q \propto \partial p_n \tag{15}$$

Although this simplified analysis neglects the interaction among the fictitious heat sources $\partial q(t)$, it shows that $\partial q(t)$ is equivalent and proportional to the deviation from the linearized contact pressure, for at least a certain range of p_n.

To implement the concept of fictitious heat sources FCHS and to include it in the framework of real-time control of thermal deformation of nonlinear machine tool structures, the time-varying strength of the FCHS $\partial q(t)$ needs to be estimated, in real time, using an inverse solution. A thermal deformation model should then be used to relate $\partial q(t)$ to the thermal deformation $\delta(x,y,z,t)$ of the structure. The formulation of these two nonlinear models and their equivalent transfer functions are developed in the following sections.

Real-time Estimation of the Fictitious Contact Heat Sources

As discussed earlier, the solution of a conventional inverse heat conduction problem IHCP requires the measurement of the temperature difference at two point near the heat source. This eliminates the contributions of other heat sources to the measured temperature. In the IHCP solution of a fictitious heat source, the temperature measurement is not an absolute temperature, but rather a deviation ∂T from a reference temperature T_{ref}. The latter is determined form the solution of the equivalent linear structure, in which the joint effect is ignored. The real time solution of this IHCP poses some unique problems that must be carefully addressed:

1. Due to the close proximity of the fictitious hear sources, they strongly interact and therefore the temperature deviation ∂T at each of the measured points is the superposition of the contribution from all of the FCHS. Under these conditions, it is impossible to estimate any one source independently of the others, making the solution of this ill-posed IHCP not unique.
2. It is not possible to activate the FCHS one at a time; they must be activated together by the main sources Q(t), producing a mixture of temperature responses at the same point in space. There is no information contained in the measured temperature data to indicate the relative contribution from each source. The temperature rise at a point near one contact source may be the result of heat generation by that source or it may be a delayed response to the heat generation of another, more distant source.
3. The magnitude of the temperature deviation ∂T at locations near the joint is of the order of one 1^oC, as will be seen in section 5.3. Therefore, the disruptive effect of the measurement noise is potentially more significant.

The non-uniqueness of the problem, and the insufficient conditions required to identify each of such unusual FCHS separately will be overcome by applying the theory of *generalized modeling*. The inherent advantage of the generalized model is that its mathematical form is similar to the mathematical form of the actual physical system. The missing information regarding the relative contribution from each source at a given point is therefore built into the model before it is calibrated. The general model for the temperature profile at a point is given by Eq. 1, in which q(t) is substituted by $\partial q(t)$ representing the heat generation of one fictitious contact heat source. The temperature at any given point is the linear superposition of the temperature profiles due to each of the contact heat sources. To understand how the generalized model can break down the temperature profile into its constituent parts consider Fig. 3, which shows two measured points T_1 and T_2 near two fictitious contact heat sources $\partial q_1(t)$ and $\partial q_2(t)$. The typical temperature profiles produced by each of the sources at the measured points for a step input of the main real source Q(t) at t= 0 is also shown in the figure. It should be noted that the temperature response to the $\partial q_1(t)$ input is felt at T_1 before it is felt at T_2 because the temperature *delay* is larger at greater distances from the source. Now, if the $\partial q_1(t)$-temperature model were calibrated to produce the T_1 temperature profile shown in Fig. 3, then the temperature. This shows that the relationships between $\partial q_1(t)$ and T1, and between $\partial q_1(t)$ and T2 are not independent. The predefined mathematical relationship forces the calibration parameters to converge to the mathematically correct solution.

Copyright © 2004 by ASME

Downloaded From: https://proceedings.asmedigitalcollection.asme.org on 07/01/2019 Terms of Use: http://www.asme.org/about-asme/terms-of-use

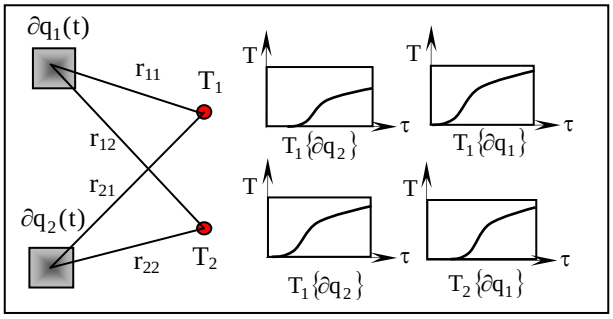

Figure 3: Schematic presentation of two fictitious contact heat sources and two temperature measurements locations

The model for the temperature rise at any point T_j on the structure is the linear superposition of the generalized models relating the q_i to T_j:

$$T_j = \sum_{i=1}^{n} T_i\{q_i, r_i\} \tag{16}$$

where the $T_i\{q_i, r_i\}$ are the generalized models corresponding to each q_i. Now, there is only one generalized model for a particular source q_i, which corresponds to Eq. 1. The same calibrated model predicts the contribution from its source onto each of the other measured points by changing the value of the parameter r in Eq. 1, called r_j in Eq. 16. In the generalized procedure for the linear problem, the variable r in Eq. 1 was treated as an ordinary empirical parameter. In the present case, the missing information in the calibration data requires that parameter r be treated as a fixed variable rather than a calibration variable. Restricting the r parameter reduces the flexibility of the generalized model to conform to the measured data, but it serves a different purpose in this case. The parameter r is used to establish the mathematical form of the system model by defining the inter-relationship between all of the temperature profiles that are produced by one contact source. The procedure used here assumes the locations of the contact sources, and then uses realistic values of the distance r from the source to the measured points. For 'm' fictitious contact heat sources there are 3m calibration parameters for the thermal model: K, a, and α for each contact source. These 3m parameters must be solved *simultaneously*, using the 'm' temperature profiles for the calibration.

Calibration of the Fictitious Contact Heat Source Model

The algorithm for calibrating the fictitious contact heat source parameters is shown in Fig. 4 for the case where m = 2. The calibrated parameters are a_1, a_2, α_1, α_2, $K_1q_1^{<1>}$, $K_1q_2^{<1>}$, $K_2q_1^{<2>}$, and $K_2q_2^{<2>}$, where the subscript indicates the heat source number and the superscript indicates the calibration input. There must be at least as many calibration inputs as there are contact sources. The calibration inputs used are step inputs

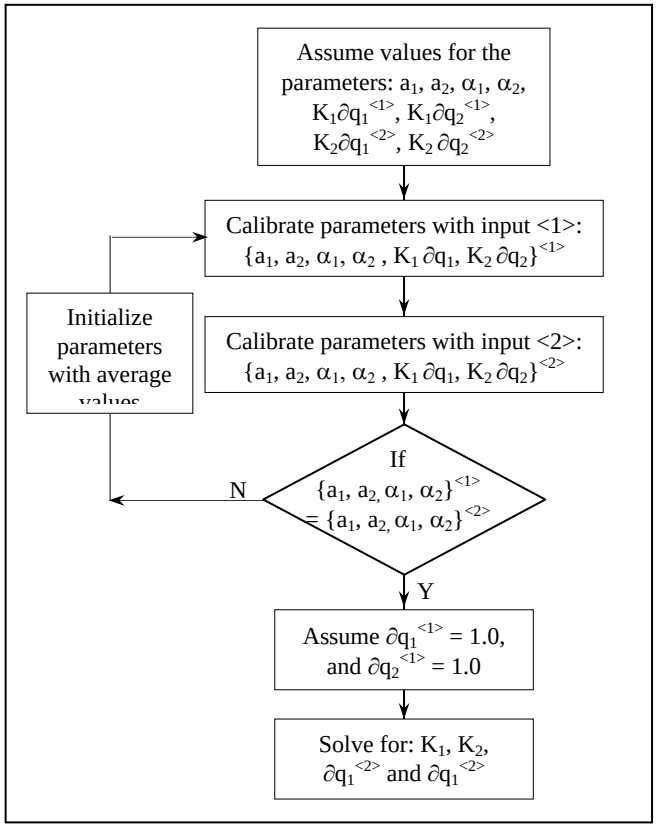

Figure 4: Flowchart for calibrating the fictitious contact heat sources

at levels smaller and greater than the reference input. The justification for treating the FCHS as step inputs when the main heat source is a step heat input is discussed in section 5.3. The first four parameters a_1, a_2, α_1, and α_2, shall be called the real parameters while the other four are called the product parameters. The first step in the calibration procedure is to assume the initial values for the four real parameters and the four product parameters. The product parameters are formed because the heat magnitudes cannot be separated from the temperature gain at this point. The next steps represent an optimization algorithm for the calibration of the <1> and <2> calibration inputs. Since the calibrated parameter values depend on the initial guess, a control loop is performed to check whether the a and α parameters are close enough to be considered equal, otherwise the two calibrated values for each parameter are averaged and the process begins again with the averaged parameter values as the initial guess. When the two calibration blocks converge to the same a and α parameters, the control moves to the next step, which assumes a reference heat magnitude of 1.0 for both $q_1^{<1>}$ and $q_2^{<1>}$, so that K_1, K_2, $q_1^{<2>}$ and $q_2^{<2>}$ may be calculated independently. Selecting reference values for the heat sources does not affect the result since the heat generation is an internal variable to the estimation transfer function.

Copyright © 2004 by ASME

Downloaded From: https://proceedings.asmedigitalcollection.asme.org on 07/01/2019 Terms of Use: http://www.asme.org/about-asme/terms-of-use

Control of the Thermal Deformation of the Machine Tool Structure

As in the linear machine tool system, the feedback signal to the control system is the vector δ(x,y,z,t), which is estimated in real time from the thermal deformation model. Therefore, the performance is the controller is proportional to the accuracy of estimating δ. The control system developed by the authors in [21] to compensate for thermal errors in multi-axis machine tools was based on a simple PID controller, with a feedforward loop. The design and performance of the system were discussed in [21,22], in terms of its dynamics, accuracy, stability, and computational efficiency. The closed loop transfer function relating the measured temperature difference ΔT(r,t) to the i^{th} axes thermal displacements, were derived [21]:

$$\frac{\delta_{i,\{d,kg\}}}{\Delta T(r,t)}(s) = \frac{G^{-1}(s)\left(D_{i,c}(s).k_g + D_{i,d}(s)\right)}{1 + D_{i,d}(s)\,P(s)} \qquad (17)$$

where P(s) is the Laplace Transform of the PID elements, while k_g is the gain of the feedforward branch. The transfer functions $D_{i,c}(s)$ and $D_{i,d}(s)$ correspond to i^{th} axis thermal displacement due to the disturbance and control heaters, Q_d and Q_c, respectively.

PREDCITION OF THE THERMAL DEFORMATION OF A NONLINEAR MACHINE TOOL STRUCTURE

Modeling of Thermal Deformation Produced by Fictitious Contact Heat Sources CHS

Once the relative magnitudes of the fictitious contact heat sources have been determined, the next step is to estimate the thermal deflection that is produced by their temperature distribution. The total thermal deflection is the superposition of the linearized thermal deformation δ_L produced by the main sources and the nonlinear deformation δ_{NL} produced by each of the contact sources. The estimation of the contribution of each of the fictitious heat sources to the overall thermal displacement is achieved through calibration of the thermal deformation models associated with each FCHS. As indicated earlier, it is not possible to activate one fictitious source at a time because any application of contact pressure in a real structure will invariably affect the entire joint. Thus, the thermal deflection models must be calibrated *simultaneously* using an error minimizing scheme. The number of calibrated inputs must be equal to or greater than the number of contact sources. Extensive computer simulation tests showed that:

1. The fourth order model used to estimate the thermal deformation of linear structure (Eq. 8) is not adequate for modeling the thermal deformation δ_{NL} produced by fictitious contact sources. A 6^{th} order model was found to give the sought for accuracy:

$$\delta_{NL}(t) = C + D - Ce^{-ct} - De^{-dt} + ETe^{-et} + Fte^{-ft} \qquad (18)$$

2. Acceptable results can be obtained when the FCHS are lumped into only two independent sources. This is so because of the close proximity of the sources and the flexibility of the generalized solution.

The Algorithm for Estimating the Thermal Deformation of a Nonlinear Machine Tool Structure using Adaptive Modeling

Figure 5 shows the algorithm for real-time application of the adaptive modeling approach to estimate the thermal deformation of a nonlinear machine tool structure. There are three sets of temperature measurements serving as the inputs to the estimation algorithm. The input Δ?T represents the temperature difference measured near any of the main sources Q(t) while T_1 and T_2 represent two measured temperatures in the vicinity of the contact joint. The first inverse solver operates on ΔT to estimate Q(t), following the procedure summarized in section 2.1 (Eq. 5). This operation is the only truly linear process since it is unaffected by the contact joint. Block 2 represents the algorithm which calculates the linearized thermal deformation model δ_L?(t), described by Eq. 8. Block 3 represents two separate algorithms, which estimate the linearized temperature profiles at T_1 and T_2 using the direct thermal model. The linearized temperatures T_{1Ln} and T_{2Ln} are subtracted from the measured temperatures T_1 and T_2 to obtain the temperature deviations ∂T_1 and ∂T_2. Blocks 4 and 5 represent the same inverse algorithm as in Block 1, now being used to estimate the disturbance heat generated by the fictitious contact heat sources ∂q_1 and ∂q_2. The estimated thermal loads are transformed into deflections δ_{NL1} and δ_{NL2} (blocks 6 and 7) and then added to the linearized thermal displacement δ_L to estimate the total displacement δ.

VALIDATION AND DEMONSTRATION OF THE ADAPTIVE MODELING APPROACH

A number of computer simulation test cases were conducted to test the validity of the nonlinear adaptive modelling approach and the accuracy of the algorithms developed in this study. The FE-based simulations also demonstrate how the proposed models are applied. The advantage of using a FE model rather than a physical test model is that it makes it possible to look at any variable in the system, even those that are inaccessible in a physical system.

Design of Numerical Simulation Experiments

A large number of FE models of machine tool structures have been investigated, using different configurations and different heat source locations, in order to identify the type of machine tool that is prone to exhibit a high degree of nonlinearity. Several general observations emerged from this study:

1) Thick-walled structures that are made of materials with higher thermal conductivity and are exposed to lower convection coefficient of heat transfer exhibit a greater degree of nonlinearity. This can be attributed to the

Copyright © 2004 by ASME

Downloaded From: https://proceedings.asmedigitalcollection.asme.org on 07/01/2019 Terms of Use: http://www.asme.org/about-asme/terms-of-use

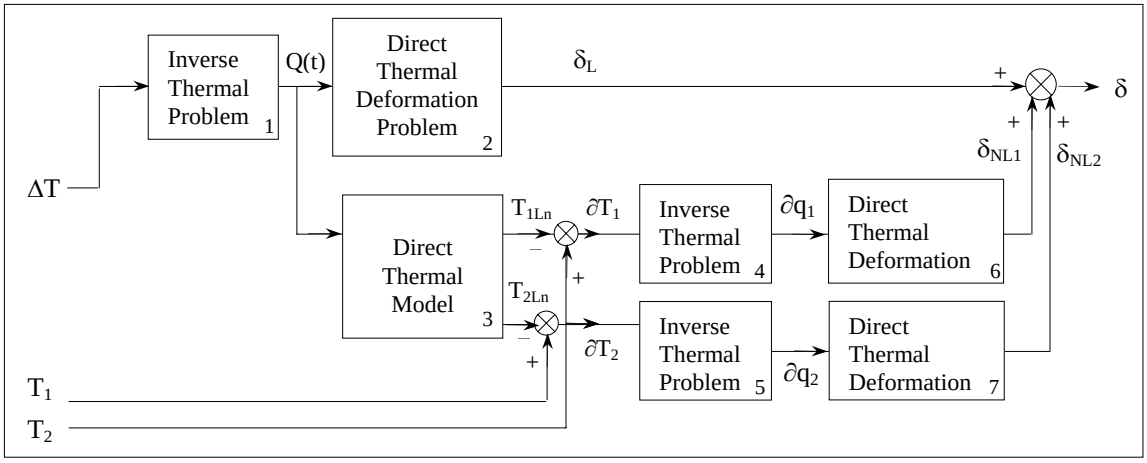

Figure 5: Block Diagram of the algorithm for estimating the thermal deformation of a nonlinear machine tool structure

the reduction of the thermal conducive resistance of the structure relative to the convective mode of heat transfer. As a result, the local temperature rise and deformation near the joint are increased.

1. The locations of the main heat sources play a critical role in controlling the system nonlinearity. Placing a heat source close to a joint has a dual effect; it increases the heat flux through the joint, and tends to increase the thermal deformation in the vicinity of the joint, which induces larger changes in the contact pressure.

Figure 6(a) shows a cross-section of a three-dimensional box-shaped FE model that was constructed using ALGOR finite-element modeling package [18]. The dimensions of the envelope containing the structure, which resembles a horizontal milling machine, are 145 x 115 x 50 cm. The contact between the column and the table takes place over two strips 40 x 7.5 cm. The structure wall thickness is 5 cm. A color enhanced solid model of the column and the contact strips, with the table removed, is shown in Fig. 6(b). Two main heat sources (Q = 90 W) that represent bearings were symmetrically placed on the inside of the column, at the base of the internal bracket. Making use of the general observations stated above, the heat sources were placed close to the contact joint, as shown in Fig. 6(b). The location of points A and B, at which thermal displacements are measured, is shown in Fig. 6(a).

The physical and thermal properties of the material are those of gray cast iron: the thermal conductivity k = 0.47 W/cm.^{o}C, the coefficient of thermal expansion $\alpha = 13.7 \times 10^{-6}$ mm/mm^{o}C, the modulus of elasticity $E = 1.04 \times 10^{5}$ MPa, and Brinell hardness $H_B = 200$. All external surfaces are exposed to convection, h = 6 kW/cm^{2} ^{o}C.

In this model, the rigidity of the support screw is simulated by using a material of $E = 2.94 \times 10^{6}$ MPa. The initial mechanical pressure is assumed to be uniformly distributed over the contact interface, $p_{c,mech} = 4.41$ MPa.

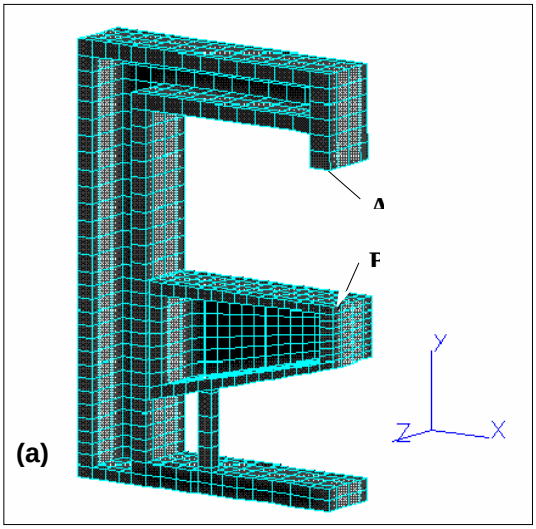

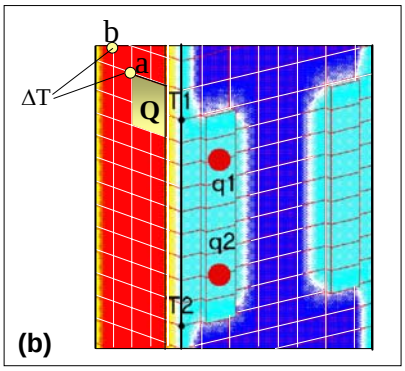

Figure 6: (a) Finite element model used for computer simulation of the nonlinear behaviour of the structure, and (b) position of the fictitious contact heat sources and temperature measurement sensors

Copyright © 2004 by ASME

Downloaded From: https://proceedings.asmedigitalcollection.asme.org on 07/01/2019 Terms of Use: http://www.asme.org/about-asme/terms-of-use

The characteristics of the contacting surfaces, which determine their stiffness and thermal contact resistance, are: standard deviation of surface roughness $\overline{\sigma}$ = 1.25 μm, and the average of the absolute slope of surface asperities $\overline{m}$ = 0.14.

Computer Simulation of the Nonlinear Thermo-elastic Behaviour of Machine Tool Structures

To simulate the system nonlinearity (Fig. 1), the results of the transient temperature field and the thermal deformation calculations are used to update the thermal contact stresses and the subsequent changes in the thermal contact resistance distribution along the joint. These new quantities and the latest temperature field are then taken as initial conditions for the next time step. This 'marching process' is repeated until the steady state is reached. For accurate predictions, a small time step of 2 seconds was used. To describe the transient response behaviour of the structure over a period of 35 minutes, these calculations are repeated nearly 1000 times. This intensive computational effort was managed by developing an algorithm that was incorporated into a general purpose FE code, ALGOR [18]. The algorithm consists of three modules and three program utilities that are integrated for automated execution of the analysis. The first 'interface element module', uses the global displacements of the interface nodes to define the global stiffness matrix [**K**], the interface conductance [**C**] as well as the nodal force vector $\{\mathbf{f}_s\}$ to be applied to the interface elements if micro-slip was detected. The [**C**] and [**K**] matrices are the assembly of their equivalent interface element matrices [**c**] and [**k**] [csme]. Given the matrix [**C**], the temperature field in the structure is obtained using the second 'thermal processor' module. The thermal deformation $\{\delta\}$ and thermal contact stresses are then determined using the third 'stress processor module'. The program modules are connected by the following three utilities. The first utility, which reads the latest [**C**], [**k**] and $\{\mathbf{f}_s\}$ matrices generated by the 'interface element module' and updates the thermal and stress finite element models. The second utility reads the nodal temperatures $\{\mathbf{t}\}$ generated by the thermal processor and writes $\{\mathbf{t}\}$ into the stress model. The third utility reads the output of the stress processor to feed the interface element module with $\{\delta\}$.

In these simulation tests, the reference step input Q_{ref} was assumed to be 295 watts, which was chosen at half the maximum thermal load. In dimensionless units, the magnitude of the reference input is $Q_{ref} = \overline{Q} = 1$. The number of the fictitious contact heat sources 'n' was taken as 2. An equal number of step inputs was also used, m = 2, for $\overline{Q}$ = 0.5 and 2. The position of the disturbance source Q, the fictitious sources q_1 and q_2, and the points of temperature measurement T_1 and T_2 are shown in Fig. 6(b).

Results and Discussion

Calibration of the linear thermal and deformation models

The first step in this analysis is to obtain the response of the nonlinear structure to $\overline{Q}$ = 1, using the algorithm described in section 5.2. The results of this analysis, which are treated as the *actual* or *measured* values, include the time variation of the following variables:

(1) the temperatures at points a, b, T1 and T2 (Fig. 6), and

(2) the relative thermal displacements between points A and B.

From the temperature difference ΔT between points 'a' and 'b', the generalized linear thermal model was calibrated (Eq. 2): with r_0 chosen as 0.12. The empirical parameters are given in Table 1, along with the parameters of the regularization function f_R (Eq. 7).

The model representing the relative thermal displacements δ(t) between points **A** and **B** (Eq. 8) was also calibrated, resulting in the empirical parameters given in Table 1. The maximum difference between the actual and calibrated curves was shown to be less than 0.1 μm.

Table 1- Calibration parameters of the linear thermal and deformation models (Eqs. 2, 7 and 8)

Thermal model	Thermal Deformation model	
	x-direction	y-direction
K= 3.372		
a=3.20	C =-0.1695	C = 3.845
α = 0.000212	D = -1.255	D = 2.355
r = 0.19	E = -.004785	E = -0.0354
Regularization parameters	c = 0.0089	c = 0.00123
A = 5.59E-03	d = 0.00129	d = 0.00142
B = 8.25E-06	e = 0.0097	e = 0.0338
γ = 0.290.		

Calibration of the nonlinear thermal and deformation models associated with fictitious heat sources

Following the procedure presented in Fig. 4, the nonlinear simulation analysis was repeated for two additional step heat inputs $\overline{Q}$ = 0.5 and 2.0 to determine the *actual* temperature rise T_1 and T_2. The temperatures were then subtracted from the temperatures estimated by the linearized FE model ($Q_{ref} = \overline{Q}$ = 1.0) to obtain the incremental temperatures ∂T_1 and ∂T_2. The calibrated parameters for the fictitious sources q_1 and q_2 are given in Table 2. The distances r_{ij} from the fictitious heat source i to the measured point j are: r_{11} = 4.89, r_{12} = 12.47, r_{21} = 10.84 and r_{22} = 6.21. These values are important because they

Copyright © 2004 by ASME

Downloaded From: https://proceedings.asmedigitalcollection.asme.org on 07/01/2019 Terms of Use: http://www.asme.org/about-asme/terms-of-use

Table 2- Calibration parameters of the linearized thermal model (Eqs. 2 and 7)

Fictitious contact source q_1	Fictitious contact source q_2
$a_1 = 0.025$ $\alpha_1 = 0.0841$ $K_1 = 3.73$ $q_1^{Q=2.0} = 2.3E\text{-}04$ $q_1^{Q=0.5} = 0.0289$ Regularization parameters $A_1 = 0.00203$ $B_1 = 7.34E\text{-}04$ $\gamma_1 = 0.0574$	$a_2 = 0.0361$ $?\alpha_2 = 0.0799$ $K_2 = 3.73$ $q_2^{Q=2.0} = 1.0$ $q_2^{Q=0.5} = -0.124$ Regularization parameters $A_2 = 0.00369$ $B_2 = 1.26E\text{-}04$ $\gamma_2 = 0.0268$

define the mathematical form of the system model. The T1 and T2 regularization parameters are also given in Table 2. To relate q_1 and q_2 to the thermal deformations δ_x and δ_y in x and y directions, respectively, four models are calibrated for the fictitious heat sources $q_1$and q_2. The calibrated parameters are given in Table 3.

Table 3- Calibration parameters of the nonlinear thermal deformation model (Eq. 18)

q1		q2	
x-direction	y-direction	x-direction	y-direction
C = 0.767	C = -0.241	C = -0.737	C = -0.111
D = 1.20	D = -6.29	D = 1.87	D = -7.27
E = -0.0145	E = 0.0357	E = -0.0135	E = -0.123
F = 0.0189	F = 0.201	F = 0.0178	F = 0.179
c = 0.00971	c = 0.00312	c = 0.0120	c = 0.0022
d = 0.00441	d = 0.00462	d = 0.00289	d = 0.00489
e = 0.00849	e = 0.0123	e = 0.0077	e = 0.0157
f = 0.0199	f = 0.205	f = 0.0191	f = 0.0201

Figure 7 shows the change in the contact pressure at each contact element, along the joint, as a function of time for a step heat input of magnitude $\overline{Q} = 2.0$. The elements are equally spaced and numbered 1 through 9, with element 9 corresponding to point T2 on Fig. 6(b). The figure shows that the contact pressures reach their steady-state values very quickly. All elements under compressive stresses (negative values) reach 75% of their steady state value within one minute after the application of the step heat input. Therefore, the contact pressure may be adequately represented as a step input by neglecting the relatively short transition region. This is important because it was shown by Eq. 15 that the magnitude of the fictitious heat source is proportional to the contact pressure. This leads to the conclusion that a reference step input to the fictitious contact heat sources can be approximately generated by applying a step input to the main source.

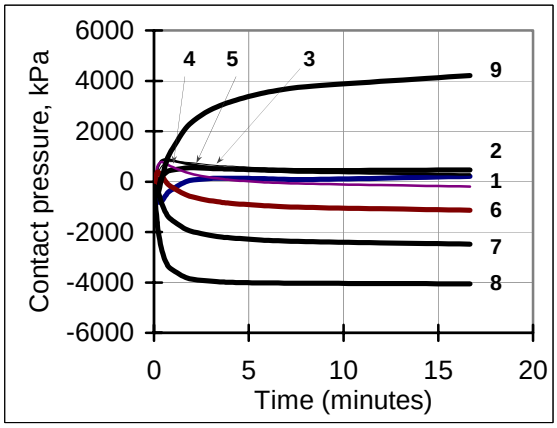

Figure 7: Change of the contact pressure distribution along the structural joint with time

Performance of the adaptive thermal deformation model

The new concept of adaptive modeling was tested for a number of non-calibrated heat input to the structure. Step heat inputs at $\overline{Q} = 1.5$ and 3.0 were chosen to test the ability of the algorithm to interpolate and extrapolate the calibration inputs. Other tests include triangular duty cycles with superimposed temperature measurement noise. These cases represent severe tests indeed, since they include abrupt change in the slope of the thermal load at the beginning, end and central transition.

For each of these test cases, the nonlinear analysis descried in section 5.2 was repeated to produce the simulated *actual measurements* of ΔT, T_1 and T_2. Referring to the block diagram representing the real-time application of the adaptive models (Fig. 5), these temperature inputs and the calibrated direct and inverse models are used to estimate the total thermal deformation, produced by the main heat sources Q and the fictitious sources q_1 and q_2. A sampling time increment of only 1 second was attainable, demonstrating the excellent computational efficiency of the adaptive models for real-time applications. This performance is exceptional, considering the fact that this nonlinear adaptive algorithm includes three inverse transfer functions, in addition to estimating the temperature at T1 and T2 that are required to calculate the temperature deviation.

Figure 8 shows the temperature deviation from the linearized thermal model for a high step input $\overline{Q}$ =3.0, at T1 and T2. Figure 9 shows the nonlinear thermal displacements δ_{NL}, which are the difference between the *actual measured* displacements δ and those predicted by the linear model δ_L. These displacements that are attributed to the structural nonlinearity may exceed 23 μm. This level of prediction error (if linear models are used) is unacceptable, considering the need of the industry to achieve a total thermal errors < $\pm$10 μm [18].

Copyright © 2004 by ASME

Downloaded From: https://proceedings.asmedigitalcollection.asme.org on 07/01/2019 Terms of Use: http://www.asme.org/about-asme/terms-of-use

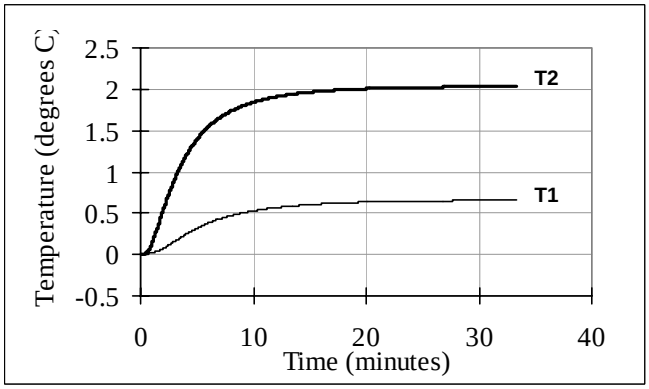

Figure 8: Temperature deviation at points T1 and T2 due to the system nonlinearity, for $\overline{Q}$ = 3.0

The thermal displacements estimated by the adaptive model are also shown in Fig. 9. The agreement between the estimated and *actual* displacement is excellent (with estimation error of < 0.5 μm) so that the two curves cannot be distinguished. For $\overline{Q}$ =1.5, better results were obtained; with estimated error of < 0.1 μm. These test cases demonstrate that the adaptive models can extrapolate beyond the calibration inputs as well as interpolate between them.

In order to simulate real operating conditions, the effect of temperature measurement noise on the accuracy and stability of the thermal deformation predictions were tested for a heat input of the form of a triangular ramp with a maximum amplitude of $\overline{Q}$ = 2.0 and a total duration of 10 minutes. A simulated measurement error was superimposed onto the resulting nonlinear temperature deviation profiles ∂T1 and ∂T2, as shown in Fig. 10. The measurement noise was generated from the actual temperature measurements taken in the experimental validation reported in [12], using thermistor probes attached to the surface of the real structure and using a high pass filter to remove the DC bias.

Figure 11 shows the estimated and *actual* nonlinear thermal displacements δ_{NL}, determined by processing the noisy temperature profiles of ∂T1 and ∂T2. The nonlinear estimation error was found to be contained within the range of ± 0.5 μm. When noiseless signal was used, the estimated error was only ± 0.15 μm. This excellent results may be somewhat surprising given the fact that the inputs to the estimation algorithm, T1 and T2, do not exceed 0.24 ^{o}C and 0.07 ^{o}C, respectively, and the range of the temperature noise is about 0.12 ^{o}C. The reason why the measurement noise is not transmitted to the output is because the thermal deflection system acts as a low pass filter [8,10,12]. This blocks the transient fluctuations in the measured temperature and transmits only the long term trend. Using the real-time estimate of the thermal deformation of the nonlinear structure as a feedback signal to the control system, the residual thermal errors are estimated to be within $\pm$3 μm, when the uncontrolled displacements are in the range of 250 μm.

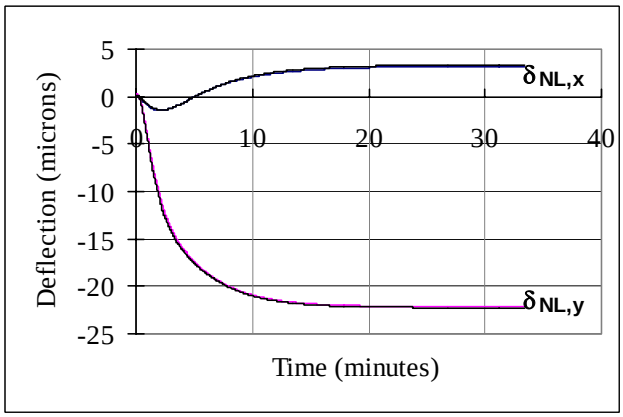

Figure 9: Actual and estimated thermal displacements due to the structure nonlinearity, for $\overline{Q}$ =3.0

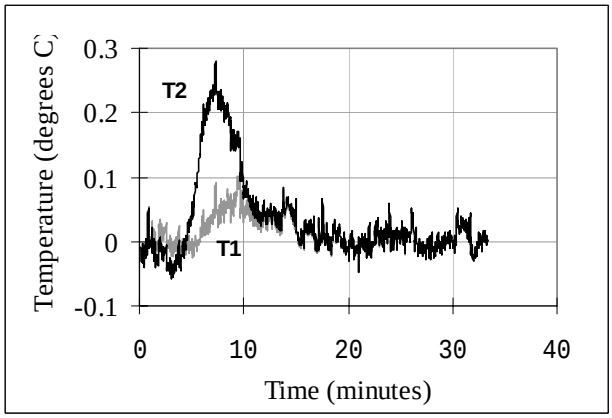

Fig. 10 Temperature deviation at T1 and T2 for the triangle heat input

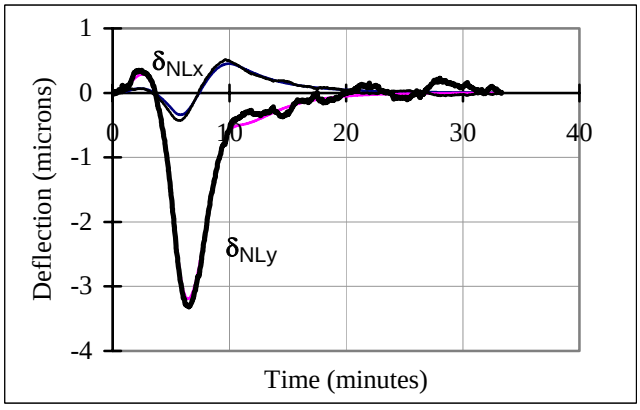

Figure 11: Actual and estimated nonlinear thermal displacements incorporating simulated temperature measurement noise

Copyright © 2004 by ASME

Downloaded From: https://proceedings.asmedigitalcollection.asme.org on 07/01/2019 Terms of Use: http://www.asme.org/about-asme/terms-of-use

CONCLUSIONS

A new concept of adaptive modeling is introduced to develop control-based dynamic models to compensate for thermal deformation of *nonlinear* machine tool structures. This concept extends the boundaries of the generalized modelling theory to solve the inverse heat conduction and thermal deformation problems of three-dimensional nonlinear complex structures in real time. A key element of the proposed adaptive modeling approach is to replace the changes in the contact pressures along the joint by fictitious contact heat sources FCHS. This approach provides a means to track the system nonlinearity through temperature measurements and real-time inverse heat conduction IHCP solution. The methodology for calibrating these fictitious sources and the algorithm of the IHCP solver were developed and demonstrated. The proposed approach dealt successfully with a number of challenges; the non-uniqueness of the problem, and the lack of sufficient conditions to identify each of such unusual FCHS separately.

Through computer simulation of the nonlinear thermoelastic behaviour of the joint, the adaptive models were tested. Results showed that the models are capable of satisfying the accuracy, stability and computational efficiency requirements for real-time applications. The models are formulated to be readily integrated with the multi-variable control system that has been developed and validated. The models are capable of estimating the thermal displacements of nonlinrear machine tool systems within $\pm$ 5 μm, in the presence of temperature measurement noise, inertia effect and the delay in the thermal response of the structure. The results also showed that the thermal deformation transfer function behaves as low-pass filters, and as such it attenuates the high frequency noise associated with temperature measurement error.

ACKNOWLEDGEMENT

The work presented in this paper was conducted under the support of the Natural Sciences and Engineering Research Council of Canada NSERC, which the authors greatly appreciate.

REFERENCES

[1] Ferreira, P.M., and Liu, C.R., 1993, “A Method for Estimating and Compensating Quasi-static Errors of Machine Tools,” ASME, J Engineering for Industry, **115**, pp. 149-159.

[2] Ni, J., and Wu, S.M., 1993, “An On-line Measurement Technique for Machine Volumetric Error Compensation,” ASME, J Engineering for Industry, **115**, pp. 85-92.

[3] Weck, M., Schuze, O., Michels, F., and Bonse, R., 1994, "Optimization of Machine Tools Performance and Accuracy," ASME Symposium on Intelligent Machine Tool Systems, Int Mech Engrg Congress and Exposition, pp.895-908.

[4] Mou, J., and Liu, C.R., 1995, “An Adaptive Methodology for Machine Tool Error Correction,” ASME J. Engineering for Industry, **117**, pp.389-399.

[5] Sata, T., Takeuchi, Y., Sakamoto, M., and Weck, M., 1981, "Improvement of Working Accuracy on NC Lathe by Compensation for the Thermal Expansion of Tool," Annals of the CIRP, **30/1**, pp. 445-449.

[6] Moriwaki, T., 1988, "Thermal Deformation and Its On-Line Compensation of Hydraulically Supported Precision Spindle," Annals of the CIRP, **37/1**, pp. 393-396.

[7] Fraser, S., Attia, M.H., and Osman, M.O.M., 1998, "Modeling, Identification and Control of Thermal Deformation of Machine Tool Structures: Part I- Concept of Generalized Modelling," ASME, J. of Manufacturing Science and Engineering, **120**, pp. 623-631.

[8] Fraser, S., Attia, M.H., and Osman, M.O.M., 1998, "Modeling, Identification and Control of Thermal Deformation of Machine Tool Structures: Part II- Generalized Transfer Functions," ASME, J. of Manufacturing Science and Engineering, **120**, pp. 632-639.

[9] Fraser, S., Attia, M.H., and Osman, M.O.M., 1999, "Modeling, Identification and Control of Thermal Deformation of Machine Tool Structures: Part III- Real Time Identification of Heat Input to the Structure," ASME, J. of Manufacturing Science and Engineering, **121**, pp. 501-508.

[10] Fraser, S., Attia, M.H., and Osman, M.O.M., 1999, "Modeling, Identification and Control of Thermal Deformation of Machine Tool Structures: Part IV- A Multi-Variable Closed-Loop Control System," ASME, J. of Manufacturing Science and Engineering, **121**, pp. 509-516.

[11] Fraser, S., Attia, M.H., and Osman, M.O.M., 1999, "Modeling, Identification and Control of Thermal Deformation of Machine Tool Structures: Part V- A Multi-Variable Closed-Loop Control System," ASME, J. of Manufacturing Science and Engineering, **121**, pp. 517-523.

[12] Fraser, S., Attia, M.H., and Osman, M.O.M., 2003, “Control-Oriented Modeling of the Thermal Deformation of Machine Tools Based on Inverse Solution of Time-Variant Thermal Loads with Delayed Response”, accepted for publication in the ASME, J. of Manufacturing Science and Engineering.

[13] Attia, M. H., and Kops, L., 1981, “System Approach to the Thermal Behaviour and Deformation of Machine Tool Structures in Response to the Effect of Fixed Joints," ASME, J. of Engineering for Industry, **103**, pp. 67-72.

[14] Attia, M.H. and Kops, L., 1979, "Nonlinear Thermoelastic Behaviour of Structural Joint - Solution to a Missing Link for Prediction of Thermal Deformation of Machine Tools," ASME, J. of Engineering for Industry, **101**, pp. 348-354.

[15] Attia, M.H. and Kops, L., "Computer Simulation of

 Copyright © 2004 by ASME

Downloaded From: https://proceedings.asmedigitalcollection.asme.org on 07/01/2019 Terms of Use: http://www.asme.org/about-asme/terms-of-use

Nonlinear Thermoelastic Behaviour of a Joint in Machine Tool Structure and Its Effect on Thermal Deformation," ASME, J. of Engineering for Industry, pp. 355-361, **101**, 1979.

[16] Attia, M.H. and Kops, L., 1980, "Importance of Contact Pressure Distribution on Heat Transfer in Structural Joints," Transactions of the ASME, Journal of Engrng. for Industry, **102**, pp. 159-167.

[17] Yovanovich, M.M., 1982, "Thermal Contact Correlations", Spacecraft Radiative Transfer and Temperature Control, T.E. Horton (ed.), Progress in Astronautics and Aeronautics, 1982.

[18] Algor Process Reference Manual, ALGOR Interactive Systems, Inc., Pittsburgh, PA.

[19] Aronson, R., 1994, “Machine Tool 101: Part 7, Machine Tools of the Future,” Manufacturing Engineering, pp. 39-45.

Copyright © 2004 by ASME

Downloaded From: https://proceedings.asmedigitalcollection.asme.org on 07/01/2019 Terms of Use: http://www.asme.org/about-asme/terms-of-use